Heliyon 10 (2024) e40758

Contents lists available at ScienceDirect

Heliyon

journal homepage: www.cell.com/heliyon

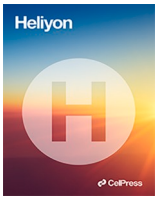

Research article

Bakuchiol from *Cullen corylifolium* and its efficacy on apoptosis and autophagy in HepG2 cells

Yeong-Geun Lee [a,1], Seon-A Jang [a,1], Hae Seong Song [a,b], Jeong Eun Kwon [a], Minsung Ko [c], Woojae Hong [c], Ahyeong Gwon [a,d], Se-Eun Park [a,d], Yujin Jeong [a], Hyunggun Kim [c,**], Se Chan Kang [a,*]

[a] *Department of Oriental Medicine Biotechnology, College of Life Sciences, Kyung Hee University, Yongin, 17104, Republic of Korea*
[b] *Kolmar Korea R&D Complex, Kolmar Korea Co. Ltd, Seoul, 06500, Republic of Korea*
[c] *Department of Biomechatronic Engineering, Sungkyunkwan University, Suwon, 16419, Republic of Korea*
[d] *Mbiometherapeutics Co., Ltd., Seongnam, 13488, Republic of Korea*

ARTICLE INFO

Keywords:
Apoptosis
Autophagy
Bakuchiol
Cell cycle arrest
Cullen corylifolia

ABSTRACT

Bakuchiol (**4**), a component of *Cullen corylifolium*, has been reported to have estrogenic, antimicrobial, and anti-inflammatory activities. Nonetheless, its anticancer mechanisms and effectiveness against hepatocellular carcinoma remain unexplored. This study sought to elucidate the mechanism of apoptosis, autophagy, and cell cycle arrest caused by bakuchiol (**4**) and three flavonoids (**1**–**3**) with similar structures to compound **4** in hepatocellular carcinoma. Among the evaluated components (**1**–**4**), bakuchiol (**4**) exhibited a significant potential to induce apoptosis in HepG2 cells. This compound facilitates apoptotic processes by engaging both intrinsic and extrinsic signaling cascades, as evidenced by the enhanced ratios of Bax to Bcl-2 and tBid to Bid. In addition, bakuchiol (**4**) induced a dose-dependent cell cycle arrest, as assessed using a Tali® image-based cytometer. Since bakuchiol decreased CDK2 and CDK4, while increasing p53, p21, and p27, these data suggest that bakuchiol regulated early cell cycle progression. It also promotes the activity of AMPK and the LC3II/LC3I ratio, while suppressing Akt and mTOR. In conclusion, these results demonstrate that bakuchiol (4), a major component of *C. corylifolium,* has an anticancer effect in hepatocarcinoma cells by inducing both apoptosis and autophagy. This significant finding enlightens us about the *potential* of bakuchiol in cancer research, particularly in liver cancer treatment.

1. Introduction

Hepatocellular carcinoma (HCC) ranks as the third most prevalent cause of cancer-related fatalities globally, with a concerning mortality rate reaching as high as 85 % in developing nations. Additionally, HCC is more prevalent in men compared to women [1]. The progression of hepatocellular carcinoma (HCC) is significantly linked to liver conditions such as cirrhosis and viral infections, particularly those caused by hepatitis B and C [2,3]. In the fight against HCC, various therapeutic and chemopreventive agents have

* Corresponding author.
** Corresponding author.
E-mail addresses: hkim.bme@skku.edu (H. Kim), sckang@khu.ac.kr (S.C. Kang).
[1] These authors contributed equally.

https://doi.org/10.1016/j.heliyon.2024.e40758
Received 16 April 2024; Received in revised form 5 November 2024; Accepted 26 November 2024
Available online 29 November 2024

been explored to induce apoptosis in response to DNA damage [4]. Natural chemotherapeutic agents, with their potential for minimal side effects, are increasingly being investigated to enhance the therapeutic efficacy for treating HCC [5,6].

Cullen corylifolium L. (Fabaceae), a traditional medicinal herb, is known for its diverse bioactivities, including antioxidant effects and scavenging activities against DPPH radicals, hydroxyl radicals, and superoxide ions [7,8]. This herb has also shown potential in reducing chemical carcinogenesis *in vivo* and inhibiting various carcinoma cell lines, such as those from the larynx, lung, and breast [9–11]. *C. corylifolium* comprises around 90 components categorized into five groups: flavonoids, coumarins, meroterpenes, benzofurans, and others [12,13].

In our previous research, we observed that apoptosis occurs in HepG2 cells induced by *C. corylifolium*. To ascertain the component responsible for this effect, we assessed the apoptosis-inducing activity of four components: psoralen, psoralidin, bavachalcone, and isobavachalcone. Despite the relatively low concentration of bavachalcone in *C. corylifolium*, it was shown to stimulate both apoptosis and autophagy [14]. Bakuchiol (**4**), one of the major components of *C. corylifolium*, has been noted for its estrogenic activity and cytotoxic effects against cancer cells [15,16]. However, detailed information regarding its specific roles in inducing autophagy, apoptosis, and cell cycle arrest is still limited.

Autophagy is an adaptive response to starvation or stress, involving the formation of autophagosomes that degrade cellular organelles to produce energy [17]. While autophagy supports cell survival, it also has a complex relationship with programmed cell death [18]. Recent investigations indicate that autophagic programmed cell death (PCD) plays a significant role in cellular demise, leading to increased research focused on the relationship between autophagy and apoptosis [19,20]. Based on these insights into autophagy, extensive research is currently underway to develop novel anticancer therapies [21,22].

Therefore, this research seeks to explore the effects of bakuchiol (**4**), the most abundant active component in *C. corylifolium*, on apoptosis and autophagy, and to elucidate the underlying signaling pathways.

2. Materials and methods

2.1. Plant materials

Dried *C. corylifolia* samples were obtained from a pharmaceutical market in Daegu, Korea, in April 2018 and authenticated by Professor Se Chan Kang at Kyung Hee University, Yongin, Korea. A voucher specimen (KHU-BMRI-201804) was deposited at the Bio-Medical Research Institute, Kyung Hee University, Yongin, Korea.

2.2. General experimental procedures

The CYTO-ID Autophagy Detection Kit was obtained from Enzo Life Sciences (Farmingdale, NY, USA). The Tali® Cell Cycle and Apoptosis Kits were acquired from Thermo Fisher Scientific in Waltham, MA, USA. Antibodies against p53, p21, p27, and CDK2 were sourced from Santa Cruz Biotechnology (Santa Cruz, CA, USA), while those targeting Bax, Bcl-2, Bid, Caspase 3, PARP, *p*-AMPK, AMPK, *p*-Akt, Akt, *p*-mTOR, mTOR, LC3 I/II, and β-actin were procured from Cell Signaling Technology (Danvers, MA, USA). The CDK4 antibody was purchased from Abcam (Cambridge, MA, USA). All compounds, including isoneobavaisoflavone (**1**), neobavaisoflavone (**2**), bakuchalcone (**3**), and bakuchiol (**4**), were acquired from ChemFaces (Wuhan, Hubei, China), each exhibiting a purity greater than 98 %. For the separation of major components, thin layer chromatography (TLC) was performed using Kiesel gel 60F254 and RP-18 F254s plates (Merck). Visualization of spots on the TLC plates was achieved with a Spectroline Model ENF-240 C/F UV lamp (Spectronics Corporation, Westbury, NY, USA) after spraying with a 10 % H_2SO_4 solution and subsequent heating. Nuclear Magnetic Resonance (NMR) spectra were recorded on a Bruker Advance 600 instrument (Bruker, Billerica, MA, USA). HPLC-grade acetonitrile and water were sourced from Burdick & Jackson (Muskegon, MI, USA), while all other reagents were obtained from Sigma-Aldrich (St. Louis, MO, USA).

2.3. Structural elucidation of bakuchiol

A dried sample of *C. corylifolia* (10 g) underwent extraction with 70 % ethanol at ambient temperature over 24 h. The resulting *C. corylifolia* ethanol extract (CCE) was subsequently concentrated under vacuum conditions. Bakuchiol (**4**), identified as the predominant compound within CCE, was isolated through semi-preparative high-performance liquid chromatography (HPLC) utilizing a Waters 600S system (Waters, Milford, MA, USA), equipped with a Waters 2487 UV detector set to 245 nm. Chromatographic separation was performed on a Cosmosil 5C18 column (5 μm, 250 × 10 mm, Waters) with a mobile phase comprising 0.1 % formic acid in water (solvent A) and acetonitrile (solvent B) in a 3:7 ratio, maintained at a flow rate of 4 mL/min over 30 min. For injection, CCE was dissolved to a 10 mg/mL concentration in 80 % methanol, and 1 mL of this preparation was introduced into the HPLC system under these specified conditions. As a result, compound **4** was successfully separated at 18.925 min, and it was collected by hand repeatedly and evaporated under a vacuum.

Bakuchiol (**4**): Yellow needles (DMSO-d_6); FAB/MS *m/z* 257 $[M+H]^+$; ^{1}H NMR (600 MHz, DMSO-d_6, δ_H) 7.19 (1H, d, J = 8.4, H-10), 7.19 (1H, d, J = 8.4, H-14), 6.69 (1H, d, J = 8.4, H-11), 6.69 (1H, d, J = 8.4, H-13), 6.17 (1H, d, J = 16.2, H-8), 6.01 (1H, d, J = 16.2, H-7), 5.86 (1H, dd, J = 17.4, 10.2, H-16), 5.09 (1H, dd, J = 7.2, 7.2, H-3), 4.98 (1H, dd, J = 10.2, 1.2, H-17a), 4.95 (1H, dd, J = 17.4, 1.2, H-17b), 1.88 (2H, q, J = 7.2, H-4), 1.62 (3H, s, H-1), 1.52 (3H, s, H-15), 1.42 (2H, m, H-5), 1.14 (3H, s, H-18); ^{13}C NMR (150 MHz, DMSO-d_6, δ_C) 156.7 (C-12), 145.8 (C-16), 133.8 (C-7), 130.4 (C-2), 128.2 (C-9), 127.0 (C-10), 127.0 (C-14), 126.4 (C-8), 124.6 (C-3), 115.2 (C-11), 115.2 (C-13), 111.7 (C-17), 42.0 (C-6), 40.8 (C-5), 25.4 (C-1), 22.9 (C-18), 22.7 (C-4), 17.4 (C-15).

2.4. Quantitative analysis of phenolics in CCE

Calibration curves for the four targeted components (**1**–**4**) were constructed using 11 different concentrations in 50 % methanol, ranging from 1.953125 to 2000 μg/mL. For each injection, a 10 μL aliquot of the extract solution (10 mg/mL in 100 % methanol) was analyzed on a Waters 600S HPLC system equipped with a Waters 2487 UV detector (280 nm, Waters). The separation utilized a Shimpack Gist column (3 μm, 250 × 4.6 mm, Shimadzu Co., Kyoto, Japan). The mobile phase employed in the analysis comprised 0.1 % acetic acid in water (solvent A) and acetonitrile (solvent B). The gradient for solvent B was as follows: 40 % at 0.01 min, transitioning to 60 % at 15 min, reaching 80 % at 26 min, maintaining 80 % until 30 min, then increasing to 100 % at 35 min, and remaining at 100 % until 70 min, with an elution rate of 0.4 mL/min. Each analytical run was conducted in triplicate to ensure precision.

2.5. Cell viability assay

Human hepatocellular carcinoma HepG2 cells were cultured in Dulbecco's Modified Eagle Medium (DMEM) supplemented with 10 % fetal bovine serum (FBS) and 1 % penicillin/streptomycin. A total of 1×10^4 cells per well were treated with various concentrations of the four compounds (12.5, 25, 50, 100, and 200 μg/mL), along with doxorubicin at a concentration of 6.25 μg/mL, for 24 h. Following treatment, MTT [3-(4,5-dimethylthiazol-2-yl)-2,5-diphenyl tetrazolium bromide; Sigma-Aldrich] was introduced and incubated for 4 h. Cell viability was determined using a Multi-Reader (TECAN, Switzerland) at a wavelength of 570 nm.

2.6. Western blot analysis

After two washes with cold PBS, HepG2 cells were lysed using PRO-PREPTM Protein Extraction Solution (iNtRON Biotechnology, Sungnam, Korea) supplemented with protease and phosphatase inhibitors. The lysates were clarified through centrifugation at 13,000×*g* for 30 min at 4 °C, and protein concentrations were quantified based on a bovine serum albumin (BSA) standard curve. Equal amounts of protein were denatured at 100 °C for 5 min and subsequently separated on Mini-PROTEAN TGXTM Precast Gels. Proteins were transferred to polyvinylidene fluoride (PVDF) membranes, blocked with 5 % skim milk for 1 h, and incubated with primary antibodies overnight at 4 °C. After six washes with TBST (5 min each), the membranes were exposed to secondary antibodies at room temperature for 1 h, followed by an additional six TBST washes. Protein bands were visualized using EZ-Western Lumi Pico reagents.

2.7. Tali® image-based cytometric assay

The assessment of apoptosis in HepG2 cells was performed using a Tali® image-based cytometer (Thermo Fisher Scientific, Waltham, MA, USA), following established protocols [14]. HepG2 cells were treated with the four components (**1**–**4**) for 24 h. After treatment, cells were harvested and analyzed using the Tali® Apoptosis Kit, following the manufacturer's instructions.

2.8. Cell cycle analysis

Cell cycle distribution was analyzed utilizing the Tali® image-based cytometer (Thermo Fisher Scientific, Waltham, MA, USA), adhering to the manufacturer's guidelines. After 24 h of treatment with each of the four components, HepG2 cells were collected, suspended, and fixed overnight in 70 % ice-cold ethanol at −20 °C. Following fixation, cells were washed with PBS, stained with the Tali® Cell Cycle Solution for 30 min, and analyzed with the Tali® cytometer.

2.9. Autophagy detection

The CYTO-ID Autophagy Detection Kit (Enzo Life Sciences, Farmingdale, NY, USA) was utilized to measure autophagic vacuole accumulation and autophagic flux in live cells, according to the manufacturer's protocol. The CYTO-ID dye selectively stained autophagic vacuoles green, while nuclei were counterstained with Hoechst 33342 to visualize them in blue. Stained vacuoles and nuclei were observed using a fluorescence microscope.

2.10. Molecular docking analysis

Vascular endothelial growth factor (VEGF) acts as a primary regulator with specific activity in vascular endothelial cells. VEGF exerts its effects via three receptors, with VEGFR-2 being a key mediator of VEGF-driven angiogenesis, making it a critical target in anti-angiogenic therapies. Blocking VEGFR-2 signaling is a promising therapeutic approach to reduce tumor angiogenesis and subsequent growth. As such, VEGFR-2 was selected as the target protein for the molecular docking simulation of CCE-derived compounds.

The molecular docking simulations were conducted using AutoDock software (The Scripts Research Institute, La Jolla, CA, USA) to calculate the binding affinities between CCE-derived compounds, specifically bakuchiol and bavachalcone, and VEGFR-2. The crystal structure of VEGFR-2 (PDB ID: 3WZD) was obtained from the Protein Data Bank (PDB) at the Research Collaboratory for Structural Bioinformatics (RCSB). The three-dimensional structures of bakuchiol (4) and bavachalcone were constructed using ChemOffice (PerkinElmer, Waltham, MA, USA) and converted to PDB format via Open Babel (http://openbabel.org). Once the protein and ligand structures were prepared, all non-essential heteroatoms and water molecules were excluded, and polar hydrogens were added to each structure. Kollman and Gasteiger charges were assigned to the protein and ligand structures, respectively. Both VEGFR-2 and the

ligands were then converted to PDBQT files (Protein Data Bank, Partial Charge (Q), and Atom Type (T) format). The binding affinities between VEGFR-2 and the ligands were evaluated within the AutoDock platform.

Lenvatinib is a well-known drug that targets VEGFR-2. Detailed binding mechanisms, particularly dynamic interaction, between VEGFR-2 and lenvatinib are valuable to understand for future drug design for tumor angiogenesis. The known binding site of VEGFR-2 with lenvatinib was utilized for docking simulations of bakuchiol and bavachalcone. The docking protocol was validated through redocking of VEGFR-2 and lenvatinib. The grid parameters for docking were established at dimensions of 40 × 40 × 40 with a grid spacing of 0.375 Å, centered on the ligand's position within the binding site. A standard Lamarckian Genetic Algorithm (LGA) was utilized to optimize docking, and the conformations with the highest negative binding energies were identified upon completion of the docking process.

2.11. Statistical analysis

Results are expressed as mean ± standard error of the mean (SEM). Differences among groups were analyzed using one-way analysis of variance (ANOVA), with statistical significance set at $p < 0.05$.

3. Results

3.1. Isolation and structure elucidation of bakuchiol from C. corylifolium

Dried *C. corylifolium* was extracted in 70 % aqueous EtOH, and the major components in *C. corylifolium* were purified by semi-preparative HPLC. The chemical structure of the bakuchiol (**4**), was determined on the basis of spectroscopic data such as NMR and FAB/MS (Figs. S1 and S2). Compound **4** was isolated as yellow needles and its molecular weight was determined to be 256 from the molecular ion peak *m/z* 257 $[M+H]^+$. The ^1H NMR (600 MHz, DMSO-d_6, δ_H) spectrum showed four olefin methine proton signals [δ_H 7.19 (1H, d, J = 8.4, H-10,14), δ_H 6.69 (1H, d, J = 8.4, H-11,13)], which were attributed to a *para*-substituted benzene ring. The olefin methines with *trans* configuration were also observed at δ_H 6.17 (1H, d, J = 16.2, H-8) and δ_H 6.01 (1H, d, J = 16.2, H-7). Also, three olefin methine protons [δ_H 5.86 (1H, dd, J = 17.4, 10.2, H-16), δ_H 4.98 (1H, dd, J = 10.2, 1.2, H-17a), and δ_H 4.95 (1H, dd, J = 17.4, 1.2, H-17b)] were indicating that presence of exomethylene. In addition, one olefin methine proton [δ_H 5.09 (1H, dd, J = 7.2, 7.2, H-3)], two allyl methyl proton [δ_H 1.62 (3H, s, H-1) and 1.52 (3H, s, H-15)], and one methyl proton [δ_H 1.14 (3H, s, H-18)] were also detected. The ^{13}C NMR (150 MHz, DMSO-d_6, δ_C) spectrum exhibited 18 carbons indicating compound **4** to be meroterpene, phenylethanoid with two isoprenes. One oxygenated olefin quaternary δ_C 156.7 (C-12), eight olefin methine [δ_C 145.8 (C-16), δ_C 133.8 (C-7), δ_C 127.0 (C-10), δ_C 127.0 (C-14), δ_C 126.4 (C-8), δ_C 124.6 (C-3), δ_C 115.2 (C-11), δ_C 115.2 (C-13)], two olefin quaternaries [δ_C 130.4 (C-2), δ_C 128.2 (C-9)], one exomethylene δ_C 111.7 (C-17), one quaternary δ_C 42.0 (C-6), two methylenes [δ_C 40.8 (C-5), δ_C 22.7 (C-4)], three methyls [δ_C 25.4 (C-1), δ_C 22.9 (C-18), δ_C 17.4 (C-15)] were observed. Taken together, the major component in *C. corylifolium* was revealed to be bakuchiol (**4**) (Fig. 1.).

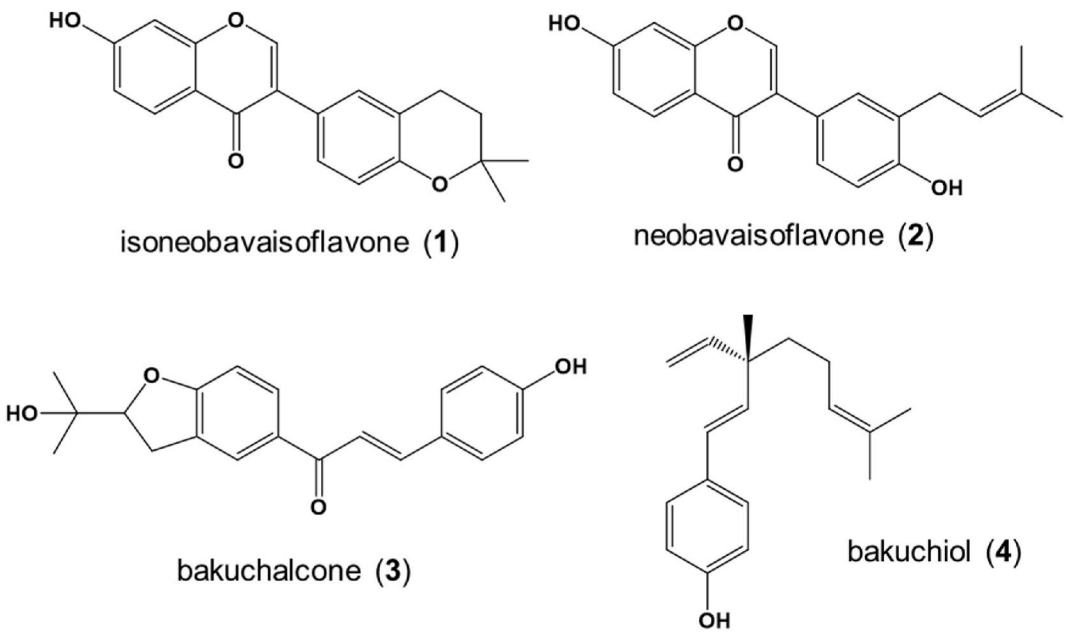

Fig. 1. Chemical structure of four components from *Cullen corylifolium*.

3.2. Quantitative analysis of phenolics from C. corylifolium

The four components (**1**–**4**) in CCE were quantified by comparing the peak areas recorded at 280 nm to calibration curves generated from standard compounds under the analytical conditions detailed in the Materials and Methods section. Also, the correlation coefficient (r^2) was 0.9999, indicating that the regression curves of each phenolic (**1**–**4**) were reliable. As a result, bakuchiol was confirmed to be a major component of CCE (11.02 ± 0.34 mg/g) (Fig. 2.).

3.3. Cell cytotoxicity of four components in HepG2 cells

To select the compound with the best cytotoxic effect among the four components (**1**–**4**), cell viability test was measured. The mean IC_{50} of isoneobavaisoflavone (**1**), neobavaisoflavone (**2**), bakuchalcone (**3**), and bakuchiol (**4**) were >200, 157.3 ± 1.13, 151.9 ± 1.97, and 70.0 ± 0.67 μg/mL, respectively (Fig. 3A). Among the four components, bakuchiol (**4**) was found the most cytotoxic to HepG2 cells. Doxorubicin was utilized as a positive control at a concentration of 6.25 μg/mL.

Subsequently, we investigated whether the four components induce apoptosis by examining specific signaling pathways associated with apoptotic induction. Following treatment with 100 μM of each component, we assessed the ratios of cleaved caspase-3 to total caspase-3 and cleaved PARP to total PARP in comparison to the control group. The ratio of cleaved caspase-3 to total caspase-3 for the four components exhibited changes of 1.08-fold, 1.02-fold, 0.97-fold, and 704.52-fold, respectively, relative to the control group. Similarly, the ratios of cleaved PARP to total PARP for the four components increased by 3.77-fold, 1.17-fold, 1.48-fold, and 16.23-fold when compared to the control group (Fig. 3B and Fig. S3). These results suggest that bakuchiol (**4**) emerges as the most potent apoptosis inducer among all components evaluated.

3.4. Effect of bakuchiol on the intrinsic and extrinsic apoptosis signaling pathways in HepG2 cells

To elucidate the mechanism underlying the apoptosis induced by bakuchiol (**4**), we investigated specific markers associated with intrinsic and extrinsic apoptosis signaling pathways (Fig. 4 and Fig. S4). The ratio of Bax to Bcl-2, which are apoptotic markers linked to the intrinsic pathway, exhibited a dose-dependent increase of 1.74-fold, 1.88-fold, and 2.24-fold in response to bakuchiol (25, 50, and 100 μM) compared to the control group. Additionally, the ratio of tBid to Bid, markers relevant to the extrinsic pathway, significantly increased by 21.64-fold at 100 μM of bakuchiol (**4**) relative to the control group. Likewise, the ratios of cleaved caspase-3 to total caspase-3 and cleaved PARP to total PARP showed remarkable increases of 52.54-fold and 165.78-fold, respectively, at the 100 μM concentration of bakuchiol (**4**) compared to the control. These findings indicate that bakuchiol (**4**) facilitates the activation of apoptosis via interaction between the intrinsic and extrinsic signaling pathways.

3.5. Effect of bakuchiol on cell cycle in HepG2 cells

To assess the impact of bakuchiol (**4**) on the cell cycle, we evaluated the various cell cycle phases (Sub G1, G0/G1, S, G2/M) utilizing a Tali® cell cycle kit. The analysis was conducted through propidium iodide (PI) staining, with the sub-G1 phase indicative of apoptotic cells that are unable to be stained due to DNA fragmentation. Prior research has indicated that cells subjected to irreversible damage undergo apoptosis, leading to an increased accumulation of cells in the sub-G1 phase [23]. Indeed, treatment with 100 μM of bakuchiol (**4**) resulted in a significant arrest of the cell cycle, elevating the proportion of cells in the sub-G1 phase from 1 % to 18 %,

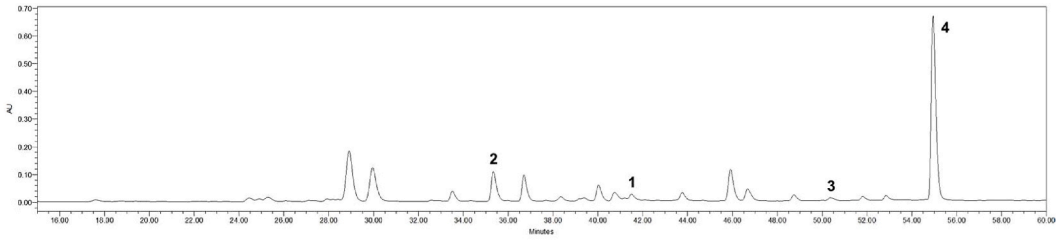

No	Retention time (min)	contents (mg/g)	regression equation
1	41.133	0.37±0.00	y=14172x+149555
2	35.232	6.91±0.09	y=14142x+631381
3	50.207	0.22±0.02	y=23577x+73647
4	54.944	11.02±0.34	y=69964x-13585

Fig. 2. HPLC chromatogram and contents of four components in 70 % EtOH extracts of *Cullen corylifolium* (CCE) (10,000 ppm). 1, isoneobavaisoflavone; 2, neobavaisoflavone; 3, bakuchalcone; 4, bakuchiol.

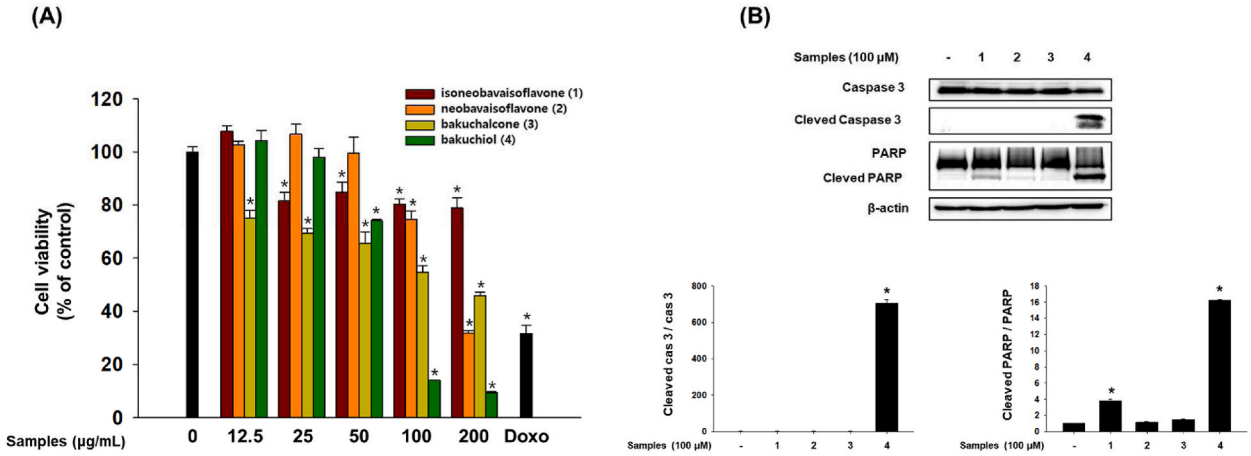

Fig. 3. (A) Evaluation of HepG2 cell viability following treatment with varying concentrations (12.5, 25, 50, 100, and 200 μg/mL) of the four components and using doxorubicin at a concentration of 6.25 μg/mL for a duration of 24 h, which acted as the positive control. Cell viability was assessed using the MTT assay. (B) Apoptotic effects of the four components on HepG2 cells treated with 100 μg/mL of each component for 24 h. 1, isoneobavaisoflavone; 2, neobavaisoflavone; 3, bakuchalcone; 4, bakuchiol. Caspase-3 and PARP expression levels were analyzed using Western blot analysis, and the densitometry results are presented as average protein expression levels. Data represent the mean ± SEM for each group, with $*p < 0.05$ indicating significance compared to the control group.

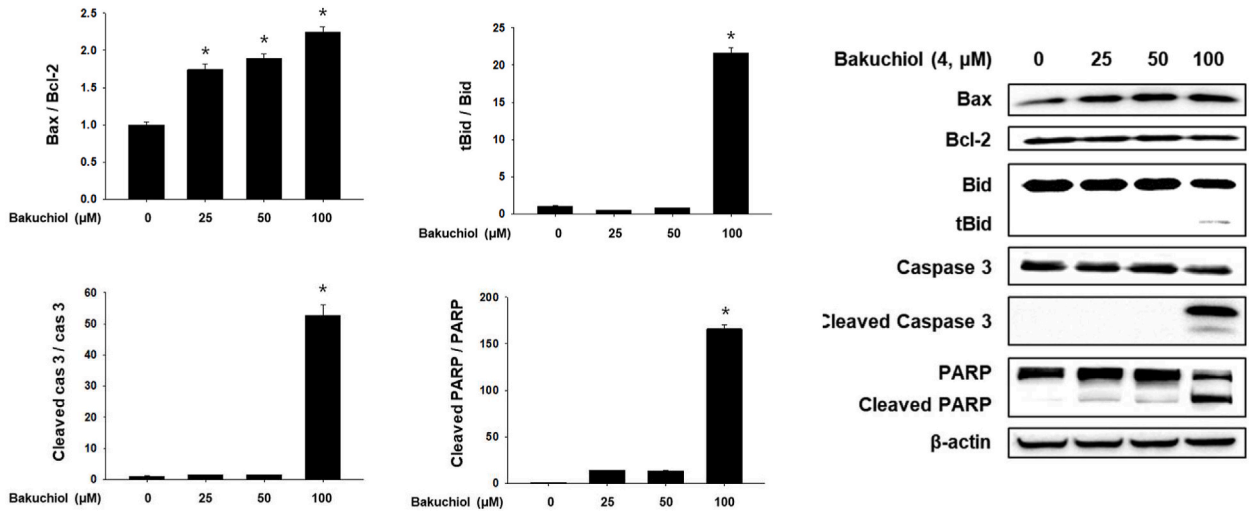

Fig. 4. Apoptotic Effects of Bakuchiol on HepG2 Cells. HepG2 cells were treated with bakuchiol at concentrations of 25, 50, and 100 μM for 24 h. The expression levels of apoptosis-related proteins, including Bax, Bcl-2, Bid, caspase-3, and PARP, were evaluated using western blotting. Densitometric analysis of the Western blot results is presented as average protein expression levels. Data are represented as mean ± SEM for each group, with statistical significance indicated by $*p < 0.05$ when compared to the control group.

and simultaneously decreasing the proportion of cells in the G2/M phase from 49 % to 30 % in comparison to the control group (Fig. 5A).

To elucidate the mechanism underlying the cell cycle arrest induced by bakuchiol (**4**), we examined key cell cycle regulatory markers, including CDK2, CDK4, p53, p21, and p27. The cyclin/CDK complex facilitates the transition to the S phase by hyper-phosphorylating Retinoblastoma (Rb) during the G1 phase [24]. Cyclin-dependent kinase inhibitors (CKIs), such as p53, p21, and p27, function to halt the cell cycle by inhibiting the cyclin/CDK complex [25]. Notably, the expression levels of p53, p21, and p27 in the bakuchiol (**4**) treatment group (100 μM) were elevated by 2.18-fold, 3.49-fold, and 2.2-fold, respectively, relative to the control group. In contrast, the expression levels of CDK2 and CDK4 were diminished by 0.27-fold and 0.14-fold at the same concentration when compared to the control group (Fig. 5B and Fig. S5).

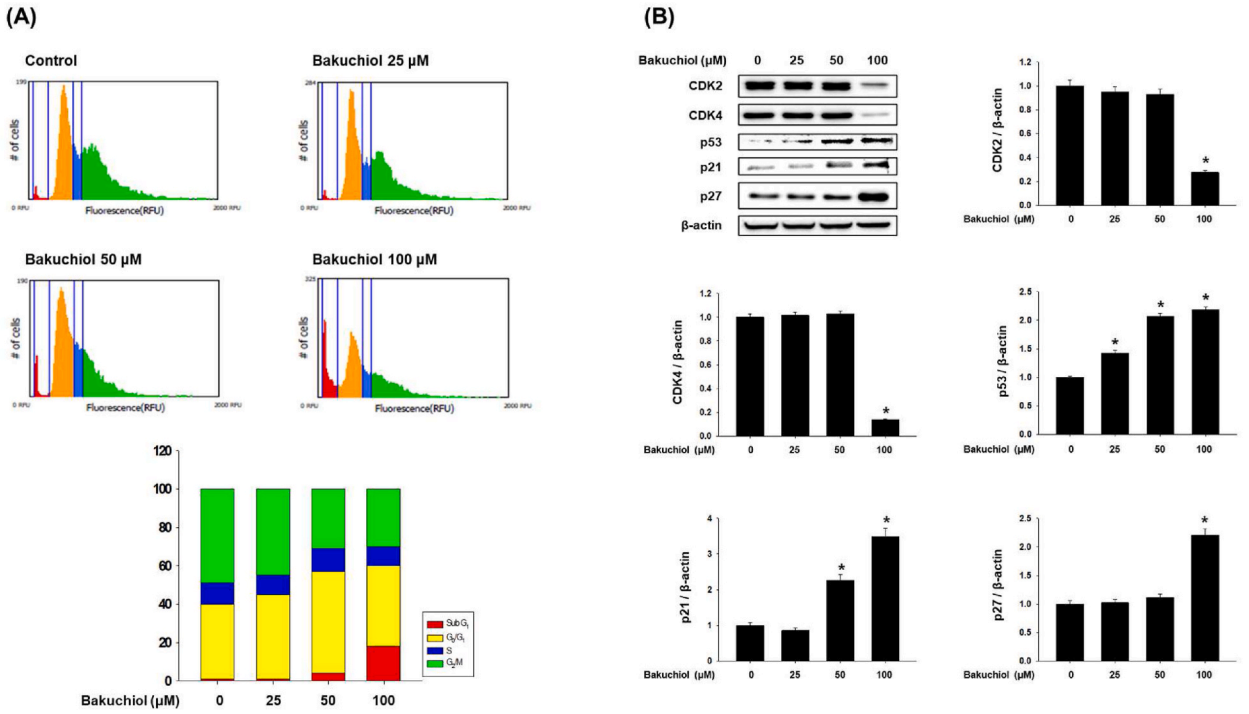

Fig. 5. Influence of bakuchiol on HepG2 cell cycle progression. (A) The distribution of cells across various phases of the cell cycle (Sub G1, G0/G1, S, G2/M) was analyzed using a Tali® image-based cytometer, assessing the effect of bakuchiol on the cell cycle in HepG2 cells treated with 25, 50, and 100 μM of bakuchiol for 24 h. (B) Western blot analysis of cell cycle regulators CDK2, CDK4, p53, p21, and p27. Densitometry data are presented as mean protein expression. Results are expressed as mean ± SEM for each group, with $*p < 0.05$ indicating significance compared to the control group.

3.6. *Effect of bakuchiol on autophage in HepG2 cells*

The Akt-mTOR signaling pathway functions as a negative regulator of autophagy, while AMPK serves as a positive regulator of this cellular mechanism [26,27]. To evaluate the role of bakuchiol (**4**) in autophagy induction in HepG2 cells, we analyzed the phosphorylation levels of Akt, mTOR, and AMPK. Treatment with compound **4** at a concentration of 100 μM resulted in a significant elevation of the phosphorylated AMPK to total AMPK ratio (1.33-fold), while concurrently reducing the ratios of phosphorylated Akt to total Akt (0.16-fold) and phosphorylated mTOR to total mTOR (0.23-fold) relative to the control group (Fig. 6A and Fig. S6). These findings indicate that bakuchiol (**4**) facilitates autophagy by modulating the AMPK and Akt-mTOR signaling pathways.

We examined compound **4**, which affects the expression of LC3I/II, as a key protein that makes autophagosomes. We found that bakuchiol (**4**) transformed LC3I into LC3II, and the ratio of LC3II to LC3I (8.06-fold) was enhanced bakuchiol (**4**, 100 μM), compared with the control group. Additionally, to determine whether bakuchiol induces autophagic vacuole accumulation and flux, we used a CYTO-ID® Autophagy detection kit. As shown in Fig. 6B, bakuchiol (100 μM) increased the autophagic vacuole accumulation and flux. The results indicate that bakuchiol promotes autophagy through the formation of autophagic vacuoles and by influencing both negative and positive regulators of this process.

3.7. *Molecular docking of bavachalcone and bakuchiol against VEGFR-2*

Molecular docking evaluation was performed for the CCE derivatives (bakuchiol and bavachalcone) with respect to VEGFR-2 to compare binding energies and conformations. Molecular docking analysis demonstrated higher binding energy (−8.54 kcal/mol) with bakuchiol than bavachalcone (−8.00 kcal/mol). Both CCE derivatives were docked in the same binding pockets (Fig. 7A and B). Bakuchiol established a hydrogen bond (HB) with Cys919 amino acid residue (AMR) (Fig. 7C) and bavachalcone revealed HBs with Cys919 and Lys868 AMRs (Fig. 7D). Lenvatinib demonstrated HBs with Cys919 and Asp1046 AMRs. All the docked components shared the same hydrogen bonding with Cys919 residue.

4. Discussion

The initiation of apoptosis occurs through the activation of caspase 3, which is cleaved by caspase 9 [28]. Once activated, caspase 3 cleaves Poly (ADP-ribose) polymerase (PARP), resulting in DNA fragmentation and the subsequent progression of apoptosis [29].

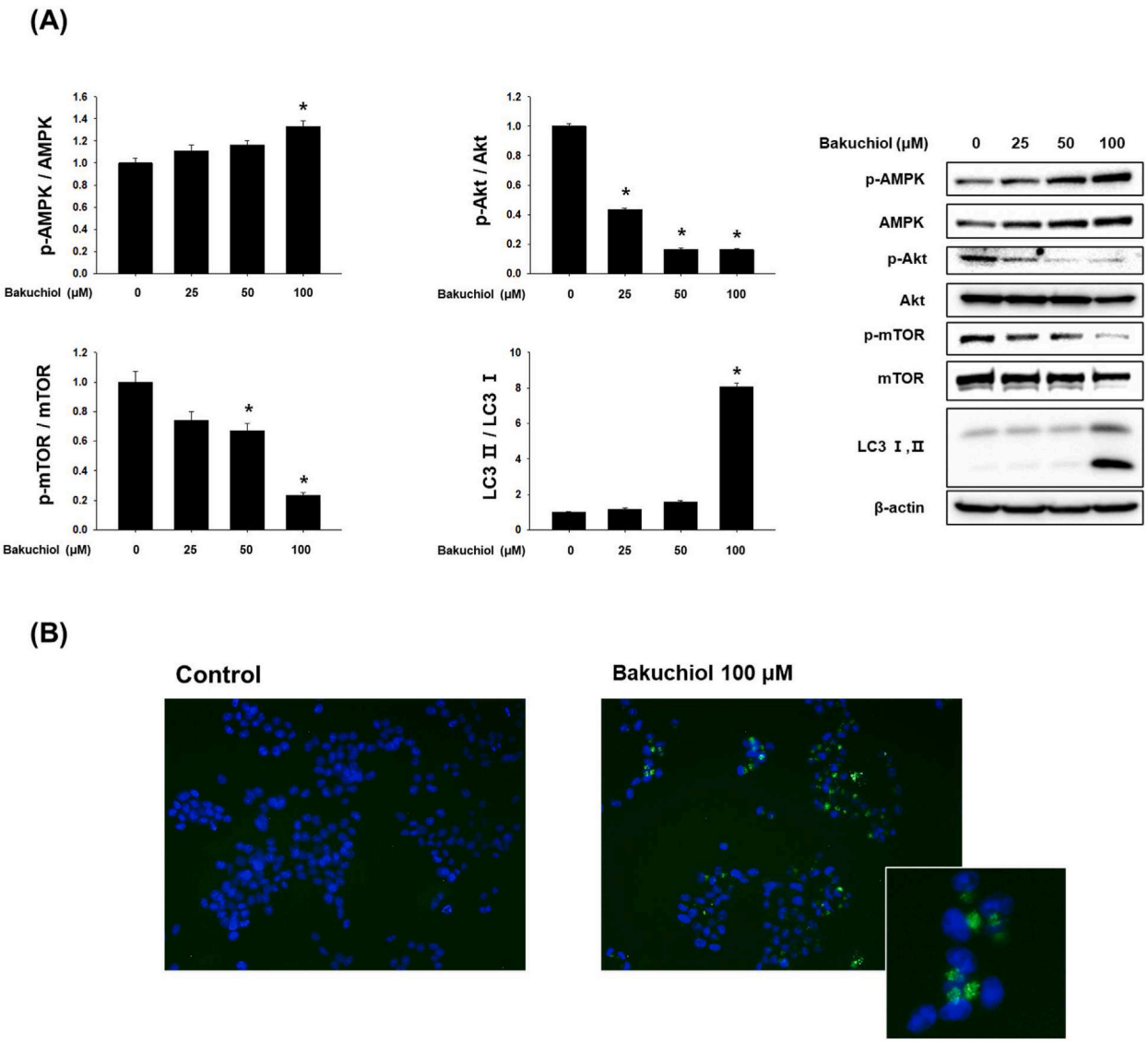

Fig. 6. Autophagic effects of bakuchiol on HepG2 cells. Cells were treated with bakuchiol at concentrations of 25, 50, and 100 μM for 24 h. (A) Western blot analysis was performed to assess the expression levels of *p*-AMPK, AMPK, p-Akt, Akt, p-mTOR, mTOR, and LC3 I/II. Densitometry results are presented as average protein expression, with data represented as mean ± SEM for each group. Statistical significance is indicated by $*p < 0.05$ when compared to control cells. (B) Visualization of autophagic vacuole accumulation and flux was conducted using the CYTO-ID® Autophagy Detection Kit. Images were captured at the original magnification of × 200.

Among the four components evaluated, bakuchiol (**4**) derived from *C. corylifolium* demonstrated significant efficacy in cleaving both caspase 3 and PARP, positioning it as a promising candidate for inducing apoptosis. Notably, this study is the first to highlight the anticancer efficacy of bakuchiol (**4**) in hepatocellular carcinoma.

The intrinsic apoptosis pathway is activated under cellular stress, where Bax translocates to mitochondria, opening the voltage-dependent anion channel (VDAC) to promote apoptosis, while Bcl-2 inhibits this process [30,31]. Our data show that bakuchiol increases the Bax/Bcl-2 ratio in a dose-dependent manner, indicating that compound **4** induces intrinsic apoptosis.

The extrinsic apoptosis pathway is triggered when a proapoptotic ligand binds to a death receptor [32]. This binding activates caspase 8, which then cleaves the C-terminal of Bid, producing tBid that migrates to mitochondria to release cytochrome *c*, leading to apoptosis [33]. Bakuchiol increases the tBid/Bid ratio, indicating that it promotes apoptosis by facilitating crosstalk between the intrinsic and extrinsic pathways.

Cell cycle regulation is crucial for cancer prevention [34]. Given the relationship between cell cycle inhibition and apoptosis, we analyzed cell cycle progression using a Tali® image-based cytometer. Our results show that bakuchiol (**4**) increases the G0 phase and decreases the G2/M phase. To further understand its mechanism, we examined cell cycle markers CDK2, CDK4, p53, p21, and p27.

During the G1 phase, CDK4 associates with cyclin D to hypophosphorylate the Retinoblastoma protein (Rb). In late G1, Rb is

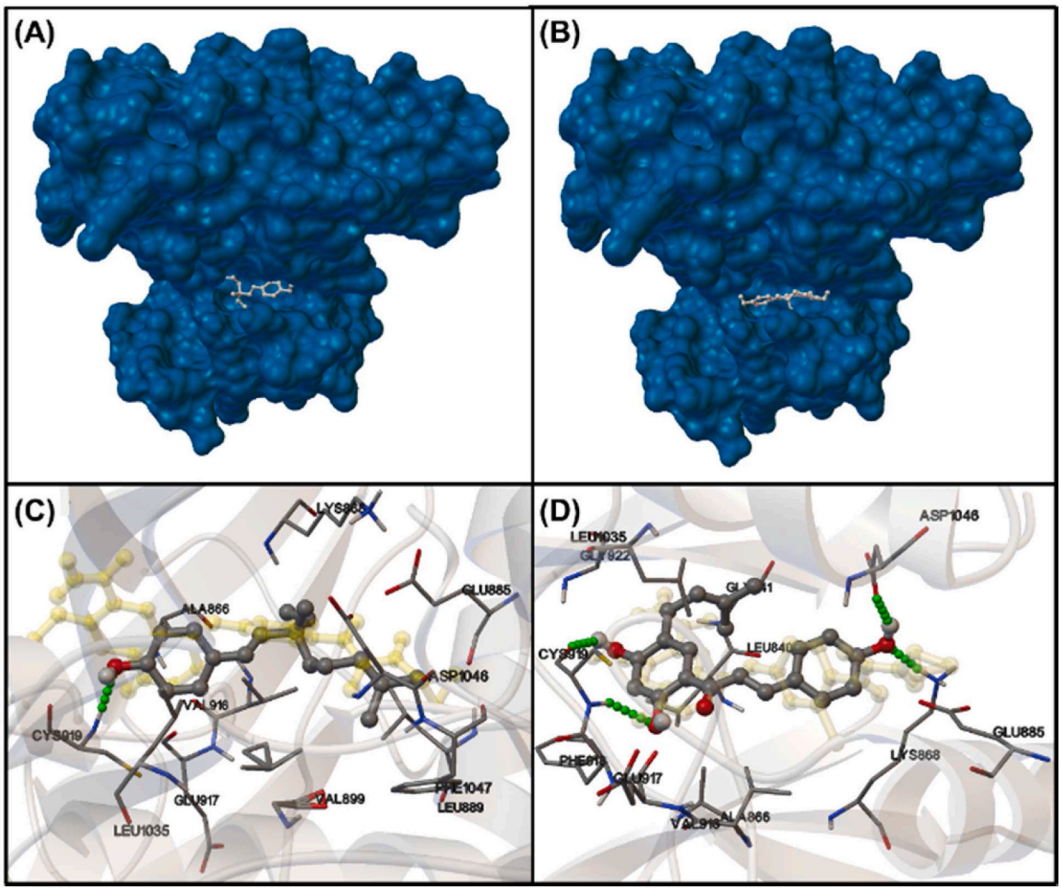

Fig. 7. Binding sites of (A) bakuchiol and (B) bavachalcone with VEGFR-2. (C) Binding between bakuchiol and VEGFR-2 (binding energy = −8.54 kcal/mol). (D) Binding between bavachalcone and VEGFR-2 (binding energy = −8.00 kcal/mol). The green dots connecting the CCE derivatives to the amino acid residue represent hydrogen bonding. Lenvatinib was displayed in transparent yellow and hydrogen bonds of lenvatinib were not shown in the figure.

hyperphosphorylated by CDK2 and cyclin E, dissociating from E2F and promoting entry into the S phase [24]. Cyclin-dependent kinase inhibitors (CKIs), including p53, p21, and p27, play a crucial role in cell cycle regulation by inhibiting the cyclin/CDK complexes [25]. Our findings demonstrate that bakuchiol (4) influences the cell cycle by upregulating the levels of p53, p21, and p27, while simultaneously downregulating CDK2 and CDK4.

In autophagy, mTOR acts as a central negative regulator [35], while PI3K/Akt inhibits mTOR and AMPK promotes autophagy [26,27]. Our findings reveal that bakuchiol enhances AMPK activity while inhibiting Akt and mTOR. LC3, a key protein in autophagosome formation, converts from its soluble form LC3I to the autophagic vesicle-associated LC3II. The increased LC3II formation in response to higher bakuchiol (**4**) concentrations indicates activation of autophagy. This was further confirmed using the CYTO-ID® Autophagy Detection Kit.

Therefore, we demonstrate bakuchiol (**4**) increases autophagy by enhancing AMPK and suppressing Akt-mTOR signaling pathway. Additional *in vivo* studies and clinical trials are imperative to substantiate the therapeutic efficacy of bakuchiol in the treatment of liver cancer.

5. Conclusion

In conclusion, this study is the first to report that bakuchiol (**4**) exhibits antitumor efficacy against HepG2 cells. Previous research indicated that *C. corylifolium* possesses anticancer activity. In our investigation, we aimed to identify which component of *C. corylifolium* is responsible for this efficacy. We discovered that compound **4**, which is present in high content in *C. corylifolium*, promotes apoptosis and autophagy. Consequently, we posit that bakuchiol (**4**) may represent a promising therapeutic candidate for the treatment of liver cancer, given its modulation of pertinent signaling pathways. Furthermore, it is imperative to conduct additional *in vivo* investigations and clinical trials to substantiate the therapeutic efficacy of bakuchiol in the context of hepatic malignancies.

CRediT authorship contribution statement

Yeong-Geun Lee: Writing – original draft, Software, Formal analysis, Conceptualization. **Seon-A Jang:** Writing – original draft, Software, Methodology, Conceptualization. **Hae Seong Song:** Software, Resources, Investigation. **Jeong Eun Kwon:** Validation, Project administration, Methodology, Investigation. **Minsung Ko:** Visualization, Software, Data curation. **Woojae Hong:** Visualization, Validation, Software. **Ahyeong Gwon:** Formal analysis, Resources. **Se-Eun Park:** Formal analysis, Resources. **Yujin Jeong:** Formal analysis, Resources. **Hyunggun Kim:** Writing – review & editing, Visualization, Conceptualization. **Se Chan Kang:** Writing – review & editing, Supervision, Project administration, Conceptualization.

Ethical approval statement

Not applicable.

Human experiments

Not applicable.

Clinical trial

Not applicable.

Data availability statement

The datasets used and/or analyzed during the current study are available from the corresponding author (S.C.K.) upon reasonable request.

Animal experiments

Not applicable.

Funding

This research was supported by a 2019 research grant (20192129) from Kyung Hee university.

Declaration of competing interest

The authors declare that they have no known competing financial interests or personal relationships that could have appeared to influence the work reported in this paper.

Acknowledgements

Not applicable.

Appendix A. Supplementary data

Supplementary data to this article can be found online at https://doi.org/10.1016/j.heliyon.2024.e40758.

References

[1] R. Siegel, D. Naishadham, A. Jemal, Cancer statistics, CA Cancer J. Clin. 63 (1) (2013) 11–30, https://doi.org/10.3322/caac.21166.
[2] C.L. Lin, R.N. Chien, C. Yeh, C.W. Hsu, M.L. Chang, Y.C. Chen, C.T. Yeh, Significant renoprotective effect of telbivudine during preemptive antiviral therapy in advanced liver cancer patients receiving cisplatin-based chemotherapy: a case-control study, Scand. J. Gastroenterol. 49 (12) (2014) 1456–1464, https://doi.org/10.3109/00365521.2014.962604.
[3] F. Donato, P. Boffetta, M. Puoti, A meta-analysis of epidemiological studies on the combined effect of hepatitis B and C virus infections in causing hepatocellular carcinoma, Int. J. Cancer 75 (3) (1998) 347–354, https://doi.org/10.1002/(SICI)1097-0215(19980130)75:3<347::AID-IJC4>3.0.CO;2-2.
[4] J.F. Kerr, A.H. Wyllie, A.R. Currie, Apoptosis: a basic biological phenomenon with wide-ranging implications in tissue kinetics, Br. J. Cancer 26 (4) (1972) 239–257, https://doi.org/10.1038/bjc.1972.33.
[5] D.S. Mandlik, S.K. Mandlik, Herbal and natural dietary products: upcoming therapeutic approach for prevention and treatment of hepatocellular carcinoma, Nutr. Cancer 73 (11–12) (2021) 2130–2154, https://doi.org/10.1080/01635581.2020.1834591.
[6] D. Rawat, S. Shrivastava, R.A. Naik, S.K. Chhonker, A. Mehrotra, R.K. Koiri, An overview of natural plant products in the treatment of hepatocellular carcinoma, Curr. Med. Chem. Anticancer 18 (13) (2018) 1838–1859, https://doi.org/10.2174/1871520618666180604085612.

[7] R. Arora, A.S. Dhaker, M. Adhikari, J. Sharma, R. Chawla, D. Gupta, A. Zheleva, Y. Karamalakova, R. Kumar, R.K. Sharma, A. Sharma, S. Sultana, R.K. Sharma, R.P. Tripathi, V. Gadjeva, Radical scavenging and radiomodulatory effects of *Psoralea corylifolia* Linn. Substantiated by *in vitro* assays and EPR spectroscopy, Z. Naturforsch., C: J. Biosci. 66 (1–2) (2011) 35–46, https://doi.org/10.1515/znc-2011-1-206.

[8] R.N. Gacche, N.A. Dhole, Profile of aldose reductase inhibition, anti-cataract, and free radical scavenging activity of selected medicinal plants: an attempt to standardize the botanicals for amelioration of diabetes complications, Food Chem. Toxicol. 49 (8) (2011) 1806–1813, https://doi.org/10.1016/j.fct.2011.04.032.

[9] P.G. Latha, K.R. Panikkar, Inhibition of chemical carcinogenesis by *Psoralea corylifolia* seeds, J. Ethnopharmacol. 68 (1999) 295–298, https://doi.org/10.1016/S0378-8741(99)00062-8.

[10] L. Whelan, M. Ryan, Ethanolic extracts of *Euphorbia* and other ethnobotanical species as inhibitors of human tumour cell growth, Phytomedicine 10 (Suppl 4) (2003) 53–58, https://doi.org/10.1078/094471103321648665.

[11] V. Rajan, J. Tripathi, P. Variyar, B.N. Pandey, Mechanism of cytotoxicity by *Psoralea corylifolia* extract in human breast carcinoma cells, J. Environ. Pathol. Toxicol. Oncol. 33 (3) (2014) 265–277, https://doi.org/10.1615/JEnvironPatholToxicolOncol.2014011391.

[12] F. Alam, G.N. Khan, M.H.H.B. Asad, *Psoralea coryliforla* L: ethnobotanical, biological, and chemical aspects: a review, Phytother Res. 32 (4) (2018) 597–615, https://doi.org/10.1002/ptr.6006.

[13] L. Chen, S. Chen, P. Sun, X. Liu, Z. Zhan, J. Wang, *Psoralea corylifolia* L: a comprehensive review of its botany, traditional uses, phytochemistry, pharmacology, toxicology, quality control and pharmacokinetics, Chin. Med. 18 (1) (2023) 4, https://doi.org/10.1186/s13020-022-00704-6.

[14] H.S. Song, S. Jang, S.C. Kang, Bavachalcone from *Cullen corylifolium* induces apoptosis and autophagy in HepG2 cells, Phytomedicine 40 (2018) 37–47, https://doi.org/10.1016/j.phymed.2017.12.030.

[15] D. Xin, H. Wang, J. Yang, Y.F. Su, G.W. Fan, Y.F. Wang, Y. Zhu, X.M. Gao, Phytoestrogens from *Psoralea corylifolia* reveal estrogen receptor-subtype selectivity, Phytomedicine 17 (2) (2010) 126–131, https://doi.org/10.1016/j.phymed.2009.05.015.

[16] S.Y. Ryu, S.U. Choi, C.O. Lee, O.P. Zee, Antitumor activity of *Psoralea corylifolia*, Arch. Pharm. Res. 15 (4) (1992) 356–359, https://doi.org/10.1007/BF02974112.

[17] B. Levine, D.J. Klionsky, Development by self-digestion: molecular mechanisms and biological functions of autophagy, Dev. Cell 6 (2004) 463–477, https://doi.org/10.1016/S1534-5807(04)00099-1.

[18] Y. Tsujimoto, S. Shimizu, Another way to die: autophagic programmed cell death, Cell Death Differ. 12 (Suppl 2) (2005) 1528–1534, https://doi.org/10.1038/sj.cdd.4401777.

[19] L. Galluzzi, E.H. Baehrecke, A. Ballabio, P. Boya, J.M. Bravo-San Pedro, F. Cecconi, A.M. Choi, C.T. Chu, P. Codogno, M.I. Colombo, A.M. Cuervo, J. Debnath, V. Deretic, I. Dikic, E.L. Eskelinen, G.M. Fimia, S. Fulda, D.A. Gewirtz, D.R. Green, M. Hansen, J.W. Harper, M. Jaattela, T. Johansen, G. Juhasz, A. C. Kimmelman, C. Kraft, N.T. Ktistakis, S. Kumar, B. Levine, C. Lopez-Otin, F. Madeo, S. Martens, J. Martinez, A. Melendez, N. Mizushima, C. Munz, L. O. Murphy, J.M. Penninger, M. Piacentini, F. Reggiori, D.C. Rubinsztein, K.M. Ryan, L. Santambrogio, L. Scorrano, A.K. Simon, H.U. Simon, A. Simonsen, N. Tavernarakis, S.A. Tooze, T. Yoshimori, J. Yuan, Z. Yue, Q. Zhong, G. Kroemer, Molecular definitions of autophagy and related processes, EMBO J. 36 (18) (2017) 1811–1836, https://doi.org/10.15252/embj.201796697.

[20] D. Denton, S. Kumar, Autophagy-dependent cell death, Cell Death Differ. 26 (4) (2019) 605–616, https://doi.org/10.1038/s41418-018-0252-y.

[21] Z. Yu, H. Tang, S. Chen, Y. Xie, L. Shi, S. Xia, M. Jiang, J. Li, D. Chen, Exosomal LOC85009 inhibits docetaxel resistance in lung adenocarcinoma through regulating ATG5-induced autophagy, Drug Resist. Updates 67 (2023) 100915, https://doi.org/10.1016/j.drup.2022.100915.

[22] D. Liu, H. Zhu, C. Li, Galectins and galectin-mediated autophagy regulation: new insights into targeted cancer therapy, Biomark. Res. 11 (1) (2023) 22, https://doi.org/10.1186/s40364-023-00466-9.

[23] K. Ishikawa, H. Ishii, T. Saito, DNA damage-dependent cell cycle checkpoints and genomic stability, DNA Cell Biol. 25 (7) (2006) 406–411, https://doi.org/10.1089/dna.2006.25.406.

[24] C.J. Sherr, J.M. Roberts, CDK inhibitors: positive and negative regulators of G1-phase progression, Genes Dev. 13 (12) (1999) 1501–1512, https://doi.org/10.1101/gad.13.12.1501.

[25] T. Abbas, A. Dutta, p21 in cancer: intricate networks and multiple activities, Nat. Rev. Cancer 9 (6) (2009) 400–414, https://doi.org/10.1038/nrc2657.

[26] B.D. Manning, L.C. Cantley, AKT/PKB signaling: navigating downstream, Cell 129 (7) (2007) 1261–1274, https://doi.org/10.1016/j.cell.2007.06.009.

[27] J. Kim, M. Kundu, B. Viollet, K.-L. Guan, AMPK and mTOR regulate autophagy through direct phosphorylation of Ulk1, Nat. Cell Biol. 13 (2011) 132–141, https://doi.org/10.1038/ncb2152.

[28] P. Li, D. Nijhawan, I. Budihardjo, S.M. Srinivasula, M. Ahmad, E.S. Alnemri, X. Wang, Cytochrome c and dATP-dependent formation of Apaf-1/caspase-9 complex initiates an apoptotic protease cascade, Cell 91 (4) (1997) 479–489, https://doi.org/10.1016/S0092-8674(00)80434-1.

[29] A.I. Scovassi, G.G. Poirier, Poly(ADP-ribosylation) and apoptosis, Mol. Cell. Biochem. 199 (1–2) (1999) 125–137, https://doi.org/10.1023/A:1006962716377.

[30] Y. Shi, J. Chen, C. Weng, R. Chen, Y. Zheng, Q. Chen, H. Tang, Identification of the protein-protein contact site and interaction mode of human VDAC1 with Bcl-2 family proteins, Biochem. Biophys. Res. Commun. 305 (4) (2003) 989–996, https://doi.org/10.1016/S0006-291X(03)00871-4.

[31] V. Kirkin, S. Joos, M. Zornig, The role of Bcl-2 family members in tumorigenesis, Biochim. Biophys. Acta 1644 (2004) 229–249, https://doi.org/10.1016/j.bbamcr.2003.08.009.

[32] I. Lavrik, A. Golks, P.H. Krammer, Death receptor signaling, J. Cell Sci. 118 (2005) 265–267, https://doi.org/10.1242/jcs.01610.

[33] M.C. Wei, T. Lindsten, V.K. Mootha, S. Weiler, A. Gross, M. Ashiya, C.B. Thompson, S.J. Korsmeyer, tBID, a membrane-targeted death ligand, oligomerizes BAK to release cytochrome c, Genes Dev. 14 (17) (2000) 2060–2071, https://doi.org/10.1101/gad.14.16.2060.

[34] C. Sherr, J. Cancer cell cycles, Science 274 (5293) (1996) 1672–1677, https://doi.org/10.1126/science.274.5293.1672.

[35] T. Noda, Y. Tor Ohsumi, A phosphatidylinositol kinase homologue, controls autophagy in yeast, J. Biol. Chem. 273 (7) (1998) 3963–3966, https://doi.org/10.1074/jbc.273.7.3963.